Magnesium Manganese Oxide Nanoribbons: Synthesis, Characterization, and Catalytic Application

Jia Liu,[†,‡] Jun Cai,[‡] Young-Chan Son,[‡] Qiuming Gao,[‡,§] Steven L. Suib,*[,†,‡,∥] and Mark Aindow[†,⊥]

Institute of Materials Science and Department of Metallurgy and Materials Engineering, University of Connecticut, Unit 3136, Storrs, Connecticut 06269-3136, Department of Chemistry, University of Connecticut, Unit 3060, Storrs, Connecticut 06269-3060, and Department of Chemical Engineering, University of Connecticut, Unit 3222, Storrs, Connecticut 06269-3222

Received: April 1, 2002; In Final Form: June 25, 2002

A todorokite-type magnesium manganese oxide molecular sieve material with a morphology of nanoribbons has been synthesized using a combination of techniques consisting of a sol−gel process to synthesize a nanosized tetraethylammonium manganese oxide layered material, an ion-exchange method to prepare a thin-film Mg−buserite (Mg−OL-1) precursor, and a hydrothermal reaction to transform the Mg−buserite to nanoribbonlike Mg−todorokite (Mg−OMS-1) material. The transformation of the Mg−buserite thin films to Mg−todorokite nanoribbons has been studied using XRD and TEM. XRD data indicate that the structural transformation of Mg−OL-1 to Mg−OMS-1 is completed after hydrothermal heating at 150 °C for about 40 h and at 200 °C for less than 8 h. TEM data show that the nanoribbons form at an early stage of the hydrothermal treatment, followed by the appearance of lattice fringes. TEM data also indicate that the well-formed nanoribbonlike crystals have a uniform tunnel dimension along the *a* axis and a long-range-ordered 3 × 3 tunnel structure along the *b* axis. FESEM data show that the lengths of the nanoribbons range from a few micrometers to tens of micrometers and that the widths range from 20 to 100 nm. Elemental and average oxidation state analyses indicate a formula for the nanoribbon of $Mg_{2.11}Mn_{5.46}O_{12}{\bullet}xH_2O$. According to TGA and TPD−MS data, these nanoribbons are thermally stable up to 500 °C. The BET surface area is 81 m^2/g, which is higher than that of bulk todorokite synthesized using conventional methods. The catalytic performance of nanoribbonlike Mg−todorokite materials on converting benzyl alcohol to benzaldehyde was improved greatly as compared to that of bulk Mg−todorokite materials.

Introduction

Manganese oxide octahedral molecular sieves (OMS) and layered (OL) materials are a family of microporous materials with edge-shared and corner-shared MnO_6 octahedra that form 1D tunnel structures or layers of various sizes.[1−5] These manganese oxide materials have been used widely in catalysis, separations, chemical sensors, and batteries because of their mixed-valent manganese, large open layers or tunnels, and high surface areas.[5,6] Preparations, investigations, and applications of bulk OMS and OL materials have been extensively explored during the past decades.[1−6] Todorokite-type magnesium manganese oxide octahedral molecular sieve material (OMS-1) is one such OMS material, containing 6.9 Å × 6.9 Å tunnels (3 × 3 framework structure).[2−4] Birnessite-type manganese oxide materials (OL-1) with a 2D layered structure are key synthetic precursors for tunnel OMS-1 materials. These OMS-1 materials have good catalytic activity because of their mixed-valent manganese and large tunnel openings. To obtain higher performance from OMS-1 materials as catalysts, one of the common techniques is to increase the surface area by decreasing the particle size.

Nanosized semiconductors and transition-metal oxides exhibit unusually high surface-to-volume ratios and size-dependent electronic and optoelectronic properties. As such, they are promising materials for catalysts, battery materials, and phosphors. There has been an intense effort to study their synthesis and structure/property relationships. Among the research of these nanosized materials, 1D nanoscale structures, including nanofibers, nanowires, and nanotubes, have been stimulating the most interest because of their unique properties and potential utilization as electronic, magnetic, and optical materials, as sensors, and as effective membranes for microanalysis.[7−12] Synthesis and investigation of nanoscale manganese oxide materials with layered and tunnel structures have drawn significant attention over the past few years. Brock et al. recently developed a preparation method to synthesize colloidal manganese oxide nanoparticles with layered structures.[13] Thin films of manganese oxides and bulk semiconductive helical fibers with a cryptomelane-type (2 × 2) framework structure have been prepared using this octahedral layered (OL) structure manganese oxide as a precursor.[14] Synthesis and characterization of nanofibrous manganese oxide material with a 2 × 4 tunnel structure also have been reported recently.[15] Yang et al. reported the synthesis of microsized fibrous Mg−todorokite using a bulk Na−birnessite precursor.[16] According to their XRD data, the

* Corresponding author. E-mail: Suib@uconnvm.uconn.edu.
† Institute of Materials Science, University of Connecticut.
‡ Department of Chemistry, University of Connecticut.
§ Current address: Shanghai Institute of Ceramics, Chinese Academy of Sciences, Shanghai, People's Republic of China.
∥ Department of Chemical Engineering, University of Connecticut.
⊥ Department of Metallurgy and Materials Engineering, University of Connecticut.

10.1021/jp0208586 CCC: $22.00
Published on Web 08/28/2002

transformation from layered Mg−buserite to Mg−todorokite was incomplete with the appearance of birnessite. To our knowledge, nanoscale todorokite-type materials with long-range-ordered tunnel structures have not yet been reported.

Here we report the synthesis, characterization, and catalytic application of magnesium manganese oxide nanoribbonlike materials synthesized from a colloidal tetraethylammonium manganese oxide precursor. These materials are single phase and exhibit the todorokite structure (OMS-1) with a nanoribbonlike morphology. This synthesis is different from conventional preparations[2−5] of bulk OMS-1 materials because a nanosized colloidal precursor with organic cations (TEA^+) is used in the interlayers instead of bulk birnessite precursors with hard cations. The resultant tunnel structure of OMS-1 in the nanoribbonlike crystals is much more ordered than that of the bulk OMS-1 materials synthesized from conventional precursors (Na−birnessite). The effects of the hydrothermal heating temperature and time on the synthesis have been studied. The transformation process of the nanoribbons also was investigated using XRD and TEM. Investigations of the properties of Mg−OMS-1 nanoribbons have been performed, including characterization of the structure, morphology, elemental composition, thermal stability, and surface area. The catalytic activity of these nanoribbonlike magnesium manganese oxides in the conversion of benzyl alcohol to benzaldehyde has also been studied.

Experimental Section

1. Synthesis. A tetraethylammonium (TEA) manganese oxide precursor with a layered structure was prepared according to the sol−gel synthesis procedure described previously.[13] Briefly, a mixture of 100 mL of distilled deionized water (DDW) and 40 mL of 2-butanol was prepared, followed by the addition of 2.49 g (containing ~0.01 mol Mn) of TEA permanganate solid with vigorous stirring. The dark-purple solution was stirred at ambient temperature for another hour. A dark-red-brown sol of TEA manganese oxides ($TEAMnO_x$) was formed as the lower aqueous layer. The top layer of organic compounds was removed using a separatory funnel. A small amount of 2-butanol was left in the aqueous layer. This resultant colloidal sol was sealed in an amber glass bottle and heated at 60 °C for 24 h to produce a gel. This $TEAMnO_x$ gel was kept in the amber glass bottle at ambient temperature for further synthesis and characterization.

To synthesize the Mg−OL-1 precursor, the $TEAMnO_x$ gel was added slowly to a solution of 500 mL of 1 M $MgCl_2$ with stirring. This solution was treated with ultrasonic vibration for 10 min, followed by stirring for an additional 1 h. The ion-exchanged precipitates were washed several times with centrifugation and transferred into Teflon-lined autoclaves. To study the transformation process, the autoclaved Mg−OL-1 samples were hydrothermally heated at 120, 150, and 200 °C for different periods of time. The resulting solids were washed three times with DDW before drying at 60 °C in air.

2. Characterization. Structural analysis was conducted using powder X-ray diffraction (XRD) and electron diffraction (ED) methods. XRD data were collected on a Scintag XDS 2000 diffractometer with Cu Kα radiation. Samples were placed on glass slides when they were still wet and dried at room temperature. To confirm the tunnel structure of the OMS-1 nanoribbons, a further ion-exchange reaction on the well-formed todorokite-type product was carried out. About 0.1 g of the OMS-1 sample was stirred for 24 h in an aqueous solution containing 1 M NaCl. The resultant solid samples were washed several times and dried at 60 °C in air. The structure of the resulting product from this reaction was investigated using XRD.

Selected-area electron diffraction (SAD) data were obtained using a Philips EM420 transmission electron microscope (TEM) at 100 kV. Samples for TEM analysis were prepared by placing a drop of OMS-1 nanoribbon suspension diluted in acetone onto a holey carbon film supported by a 3-mm copper grid and allowing the solvent to evaporate. TEM bright-field (BF) images of the nanoribbons were also acquired. The morphologies of the OMS-1 nanoribbons were studied using a Zeiss DSM 982 Gemini field-emission scanning electron microscope (FESEM) with a Schottky emitter. The sample suspension in acetone was dispersed on AuPd-coated silicon chips that had been mounted onto the stainless steel sample holders using silver conductive paint.

Inductively coupled plasma−atomic emission spectroscopy (ICP−AES) analyses were carried out on a Perkin-Elmer 7-40 instrument. Powder samples were weighed and dissolved in a 1% HCl solution. The average oxidation state (AOS) of the sample was determined using a potentiometric titration method that has been described in detail elsewhere.[17] Thermogravimetric analyses (TGA) were performed using a Hi-Res TGA 2950 model thermogravimetric analyzer. TGA analysis was carried out in a N_2 atmosphere. The temperature ramp was 10 °C/min for each analysis. Temperature-programmed desorption−mass spectrometry (TPD−MS) data were collected using a furnace and an MKS-UTI PPT quadrupole residual MS gas analyzer. About 50 mg of the sample was loaded into a quartz tube. After being purged with He for 6 h, the powder sample was heated at a rate of 10 °C/min to 700 °C. The surface area was determined on a Micromeritics ASAP 2010 accelerated surface area and porosimetry system. The samples were predegassed at 200 °C for 15 h. Nitrogen gas was used as an adsorbate at liquid nitrogen temperature. Specific surface areas were calculated by the BET method.

3. Catalytic Application. To compare the performance of nanoribbonlike catalyst with that of bulk Mg−OMS-1 material, bulk Mg−OMS-1 was prepared using a conventional method reported in the literature.[3d] The oxidation of benzyl alcohol to benzaldehyde was performed using a procedure that has been described in detail elsewhere.[18] Briefly, each of the Mg−OMS-1 catalysts were dried at 110 °C overnight before the catalytic reaction to eliminate the moisture. A solution containing 1 mmol of benzyl alcohol and 10 mL of toluene was mixed with 0.05 g of the Mg−OMS-1 catalyst in a round-bottom flask. The mixture was then stirred with refluxing at 110 °C in air for 4 h. The reaction mixture was allowed to cool to room temperature. The Mg−OMS-1 catalyst was removed by filtration. The filtrate was then analyzed using GC/MS.

Results

1. Synthesis. In the first step of the three-step procedure, the dark-purple color of the solution changed to a dark-red-brown color about 20 min after tetraethylammonium permanganate solids were added to the aqueous solution containing 28% of 2-butanol. The color change indicated the reduction of Mn^{7+} in $TEAMnO_4$ to Mn^{4+} and Mn^{3+} by 2-butanol.[13] The gelation of the $TEAMnO_x$ layered material (TEA−OL-1) began a few hours after the dark-red-brown sol was heated at 60 °C and resulted in a colloidal "jelly" material. In the second step, TEA−OL-1 was transformed into the Mg−OL-1 precursor by an ion-exchange reaction. When this gel contacted the ion-exchange solution, TEA−OL-1 nanoparticles immediately formed a black suspension in the aqueous solution. The ion-exchange reaction was completed very quickly. [13b,15c] In the third step, the thin-

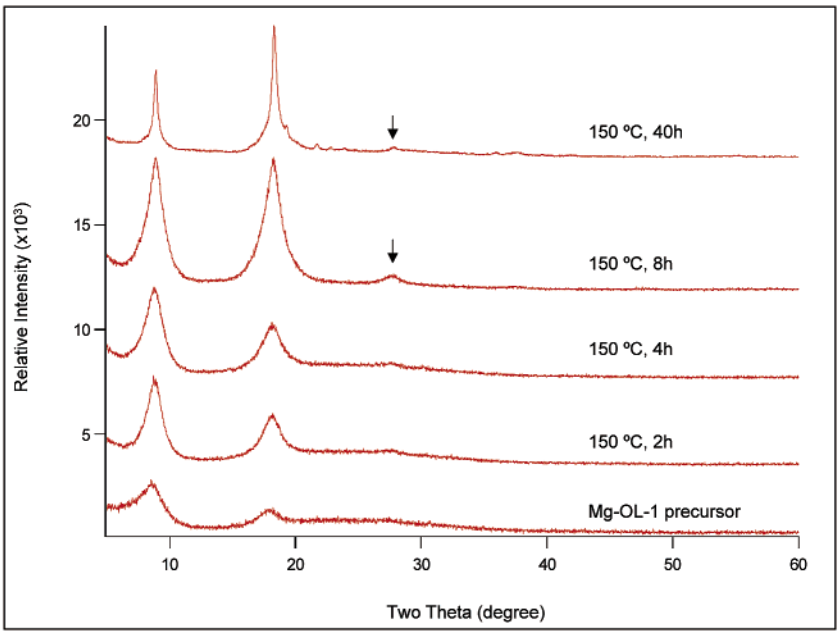

Figure 1. (Bottom trace) X-ray powder diffraction pattern of an untreated Mg−OL-1 sample, and X-ray powder diffraction patterns of Mg−OL-1 samples that were hydrothermally treated at 150 °C for 2, 4, 8, and 40 h..

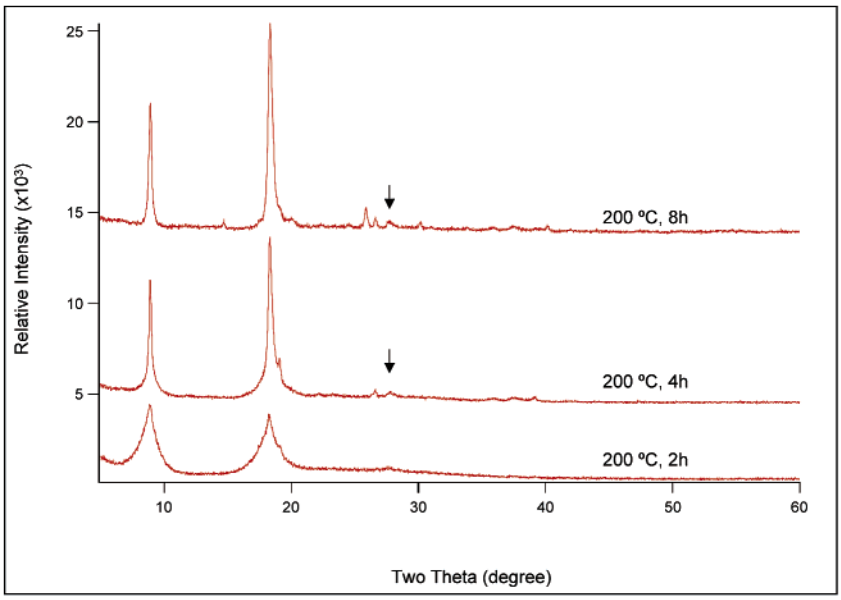

Figure 2. X-ray powder diffraction patterns of Mg−OL-1 samples that were hydrothermally treated at 200 °C for 2, 4, and 8 h.

film Mg−OL-1 was transformed into the nanoribbonlike OMS-1 material by hydrothermal heating. The OMS-1 material formed a wool-like suspension in water.

2. Transformation of Thin-Film Buserite to Nanoribbon-like Todorokite. Mg−OL-1 precursors were heated at different temperatures and for different periods of time, as described in the Experimental Section, to study the transformation of the crystal structures and the growth of the nanoribbons. The XRD data from the Mg−OL-1 samples heated at 150 °C for 2, 8, and 40 h are shown in Figure 1. Figure 2 shows the XRD data from the Mg−OL-1 samples heated at 200 °C for 2, 4, and 8 h. The basal spacings of Mg−buserite and Mg−todorokite are similar, but the different relative intensities of the peaks and the presence of additional peaks indicate the formation of todorokite from buserite. The growing intensity of the peak at 2θ near 18° is due to the formation of the todorokite structure.[2b] The XRD peaks of well-formed Mg−todorokite are sharper and much more intense than those of the Mg−buserite thin-film precursor. For well-formed todorokite, the XRD peak at 2θ of about 8° has a *d* spacing of about 9.95 Å for the (001) planes. The second large peak corresponding to the (002) planes has a *d* spacing of about 4.84 Å. These two major peaks are diagnostic peaks for todorokite.[1] Another smaller peak at 2θ of about 28° shown in the diffraction pattern has a *d* spacing of about 3.23 Å, corresponding to (003) planes, which is indicated by the arrows in Figures 1 and 2. These data are similar to reported XRD data in the literature.[2,3] At 150 °C, the transformation was completed after 40 h. At 200 °C, the transformation time was shortened to 8 h. The transformation from Mg−buserite to Mg−todorokite is faster at 200 °C than at 150 °C. The additional ion-exchange reaction described in the Experimental Section was performed on the well-formed Mg−todorokite nanoribbon samples that were heated at 150 °C for 40 h and at 200 °C for 8 h, respectively. XRD data show no shift of the todorokite peaks. At 120 °C, the conversion to Mg−todorokite was not complete after 3 days (XRD data are not shown here).

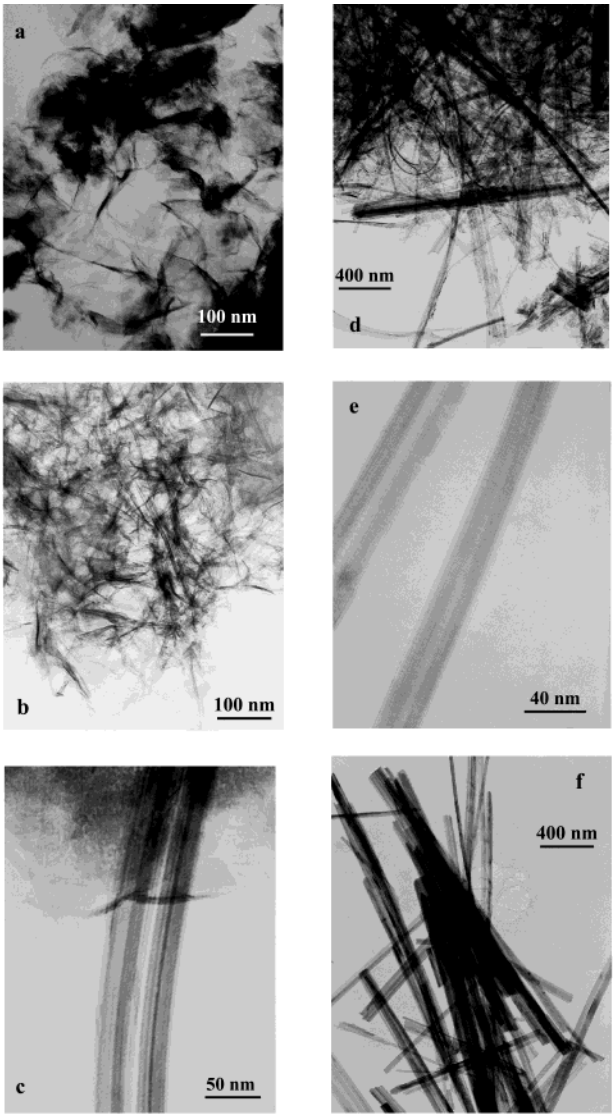

Figure 3. (a) TEM bright-field image of an untreated Mg−OL-1 sample. TEM bright-field images of Mg−OL-1 samples that were hydrothermally treated at 200 °C for (b, c) 2 h, (d, e) 4 h, and (f) 8 h.

TEM bright-field images obtained from samples with hydrothermal treatment for different time periods at 200 °C are shown in Figure 3. The Mg−OL-1 materials (Figure 3a) prepared from TEA−OL-1 have a thin-film-like morphology that is different from the bulk platelike morphology of OL-1 materials prepared using conventional methods.[1c,e, 2a,b] No twinning or dislocations have been observed in the thin-film Mg−OL-1 particles. The growth of nanoribbons was observed in the sample with hydrothermal treatment at 200 °C for 2 h. TEM images from this sample (Figure 3b,c) show a mixed morphology consisting mainly of thin films with a small amount of nanoribbon material. These ribbons are well separated from each other. No lattice fringes were observed in these ribbons (e.g., Figure 3c), which indicates that the tunnel structure of todorokite has not formed in these ribbons at this stage. The XRD pattern from this sample (Figure 2a) also confirmed that the crystalline phase was still mainly buserite. After heating at 200 °C for 4 h, the sample consisted predominantly of ribbons (Figure 3d) in which distinct lattice fringes were observed (Figure 3e). The increase of the XRD peak at 2θ near 18° (Figure 2b) indicated that a large amount of the todorokite phase had formed. After heating for 8 h at 200 °C, the Mg−OMS-1 nanoribbons were well formed.

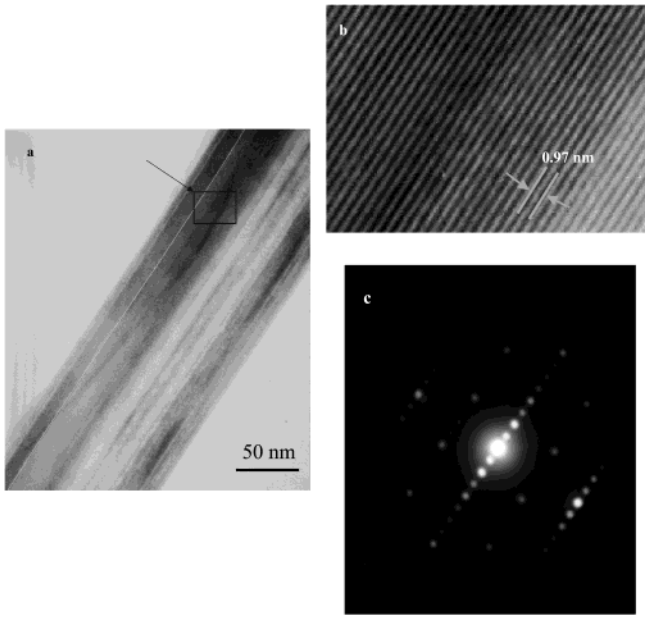

Figure 4. (a) TEM bright-field image of an OMS-1 nanoribbon prepared at 150 °C. (b) Enlarged image of the selected area in (a). A distance of 0.97 nm between fringes is shown, which corresponds to the length of the *a* axis of a unit cell. (c) Selected-area diffraction pattern of the nanoribbon in (a).

At this stage, the transformation was complete, and there was little thin-film buserite remaining in the sample (Figure 3f). The XRD data also confirmed that the transformation process was complete (Figure 2c). The peaks at 2θ values of about 14, 26, and 27° are due to manganite (γ-MnOOH).[2b] TEM bright-field images of samples autoclaved at 150 °C showed the formation of nanoribbons after heating for 4 h. In the sample heated for 8 h, there was still a noticeable amount of thin-film buserite material. After heating the sample for 40 h, the todorokite structure was well formed, and there was little thin-film material observed. The peaks at 2θ values of about 22, 23, and 24° are due to ϵ-MnO_2 (JCPDS card 12-141).

The crystallography of the OL-1 and OMS-1 nanoribbons was investigated using tilting and selected-area diffraction experiments in TEM. The surface of the nanoribbons was parallel to (001) as expected, and that of the ribbon axis was parallel to [010].

3. Crystal Structure Analysis. A TEM bright-field image of the well-formed Mg−todorokite nanoribbon prepared at 150 °C and the corresponding selected-area electron diffraction (SAD) pattern are shown in Figure 4. The lattice fringes in the enlarged image area (Figure 4b) appear at a common *a* dimension of about 0.97 nm, which corresponds to the width of the 3 × 3 tunnel. The unit cell parameters, including *a*, *b*, and β, were measured from the electron diffraction pattern in Figure 4c. The values obtained for *a* and *b* are 0.97 and 0.29 nm, respectively, and β is about 90°, which corresponds to the pseudo-orthorhombic unit cell structure of todorokite.[2] The unit cell parameters are slightly different from those reported in the literature.[1,2] The tunnels are well ordered continuously along the *b* dimension. The crystals showed little twinning and few dislocations, in contrast to the more defective todorokite materials synthesized using conventional methods.

High-resolution SEM images obtained using an FESEM microscope are shown in Figure 5. Figure 5a is an image of a typical Mg−OMS-1 nanoribbon with a width of about 70 nm. The lengths of these nanoribbons vary from a few micrometers to several tens of micrometers.

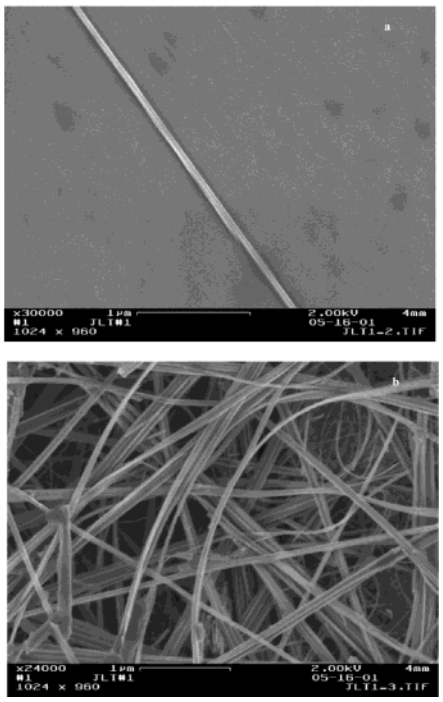

Figure 5. Morphologies of Mg−OMS-1 materials revealed by secondary electron imaging in the FESEM. (a) Image of a single OMS-1 nanoribbon. (b) Scanning image of a cross-linked OMS-1 nanoribbon nest.

The average oxidation state (AOS) of manganese ions in OMS-1 nanoribbons is 3.62, which was measured using the titration method described in the Experimental Section. The atomic ratio of Mg to Mn in OMS-1 nanoribbons determined by ICP−AES is 0.387. The elemental analysis data and AOS results indicate that the nanoribbonlike OMS-1 material has a formula of $Mg_{2.11}Mn_{5.46}O_{12}\bullet xH_2O$.

4. Thermal Stability and Surface Area. The thermal stability of OMS-1 nanoribbonlike material was studied using TGA and TPD. The TGA data for OMS-1 nanoribbons are shown in Figure 6. There are three major weight losses in the TGA profile. The first weight loss is about 5%, ranging from 40 to 130 °C. This is due to water physically sorbed on the surface. The second weight loss is about 11% from 130 °to 420 °C and is due to water escaping from the tunnels. The third weight loss, from 420 to 560 °C, is about 5% and is mainly due to oxygen evolution and structural water. TPD−MS data (Figure 7) show the evolution of oxygen from OMS-1 nanoribbon materials. The two peaks on the oxygen curve (at about 480 and 550 °C) indicate that more than one type of oxygen site exists in the structure. The peak at 550 °C is due to the evolution of lattice oxygen, and the one at lower temperature may be due to relatively active oxygen species that were absorbed in the tunnels.[3d] TGA and TPD data indicate that OMS-1 nanoribbon material is thermally stable up to 500 °C. The BET surface area of the nanoribbon sample was 81 m^2/g, which was measured using the BET method.

5. Catalytic Activity of Mg−OMS-1 Nanoribbon. Both nanoribbonlike Mg−OMS-1 and bulk Mg−OMS-1 have been used as catalysts in the oxidation of benzyl alcohol to benzaldehyde. According to the data analyzed using GC−MS, the conversion using nanoribbonlike Mg−OMS-1 catalyst was 45%, whereas the conversion using bulk Mg−OMS-1 catalyst was only 2%.

Discussion

1. Preparation of Thin-Film Mg−OL-1 Precursor. In the procedure for synthesizing todorokite nanoribbons, the first step is to prepare the thin-film Mg−buserite precursor with a layered structure. Synthetic Mg−buserite precursors are prepared conventionally by a precipitation method that results in the aggregation of birnessite-type materials, which produces larger-sized particles and twinned crystals. In these conventional methods, $KMnO_4$ or $MgMnO_4$ is used as an oxidizing reagent to synthesize layer-structured manganese oxide materials.[3] The redox reaction of $KMnO_4$ or $MgMnO_4$ and the reducing reagent is very fast, which is indicated by the immediate color change of the solution after $KMnO_4$ or $MgMnO_4$ is added to the reducing reagent. To achieve smaller-sized particles and a well-ordered birnessite-type structure, it is necessary to control the nucleation process and to prevent aggregation.

The sol−gel method provides a promising route to prepare a homogeneously mixed system of reactants to control the morphology and particle size of the product.[19,20] Compared with $KMnO_4$ or $MgMnO_4$, $TEAMnO_4$ is a much weaker oxidizing reagent. The color of the mixed solution of $TEAMnO_4$ and the reducing reagent 2-butanol changed about 20 min after $TEAMnO_4$ was added to the 2-butanol aqueous solution. The slow color change indicates that the redox reaction is slower than with conventional methods.

The slow reaction speed could prevent the precipitation and aggregation of particles that produce large particle sizes and associated twinned structures. TEA−OL-1 gel contains nanosize manganese oxide particles with layered structures, extra TEA^+ cations floating homogeneously in the matrix of water, and a small amount of 2-butanol that is dissolved in the aqueous phase, which also can prevent the precipitation and aggregation of TEA−OL-1 particles from forming larger-size particles. The use of a secondary alcohol neutral aqueous matrix instead of the aqueous salt solutions with high basicity used in conventional syntheses provides a more homogeneous environment that prevents small TEA−OL-1 particles from coagulating or condensing. The hard cations (Na, K ,or Mg) in conventional syntheses of birnessite materials have also been replaced by soft organic cations to control the condensation of the manganese oxide-layered nanocrystals.[13]

The second step is to transform the layered material into the Mg−buserite precursor by an ion-exchange reaction. Instead of smaller hard metal cations such as K^+ or Na^+ used in conventional syntheses, larger organic TEA^+ cations sit in the interlayer region of the birnessite structure. Therefore, the ion-exchange method for preparing the Mg−buserite precursor is much simpler without ion-exchange competition from hard cations. The ion-exchange reaction is completed quickly and achieves the maximum cation-exchange capacity both because of the large interlamellar spacing in TEA−OL-1 and because the positive charge of the TEA^+ cations is smaller than that of the magnesium cations.

Ultrasonic vibration is applied to prevent these layered Mg−buserite particles from aggregating as well as to accelerate the ion-exchange reaction. Thin films of Mg−OL-1 are formed after the ion-exchange step. The dark areas in Figure 3a may be due to folding of the thin-film sheets. The morphology of the resultant Mg−OL-1 particle is quite different from that of bulk Mg−OL-1 materials. Thin films are the predominant morphology of the Mg−OL-1 precursor instead of the larger twinned platelike particles that are often observed in bulk buserite materials.

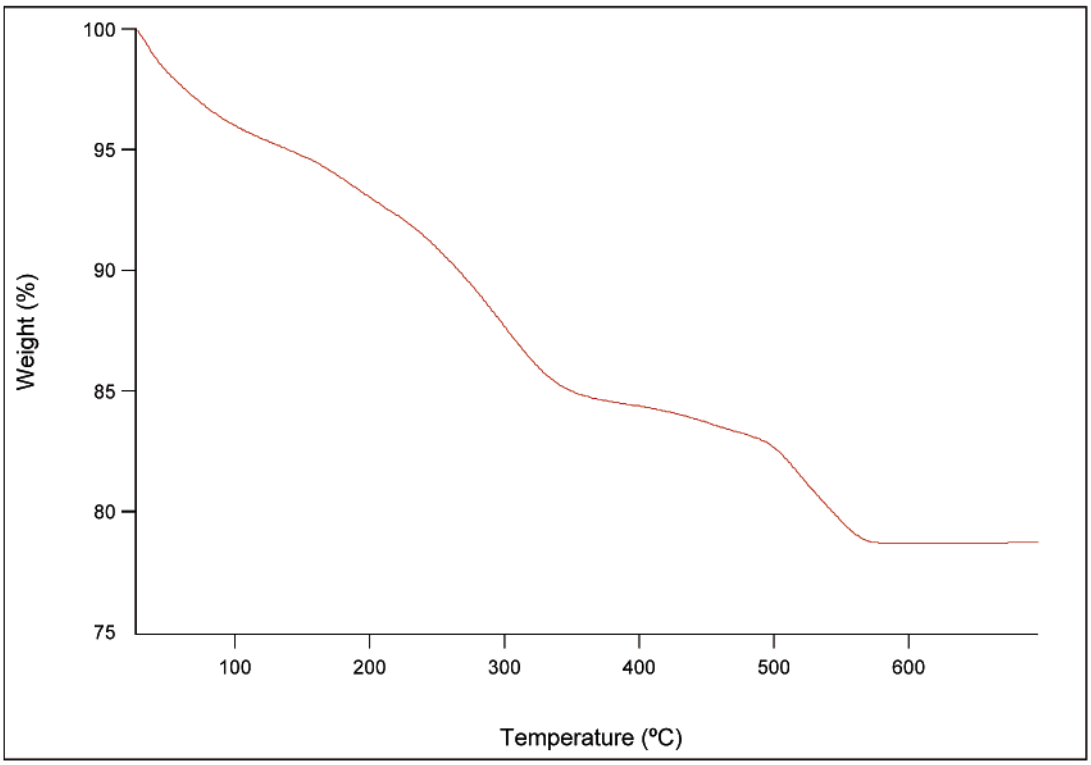

Figure 6. TGA plot for OMS-1 nanoribbons in a N_2 atmosphere from 30 to 700 °C with a ramp of 10 °C/min.

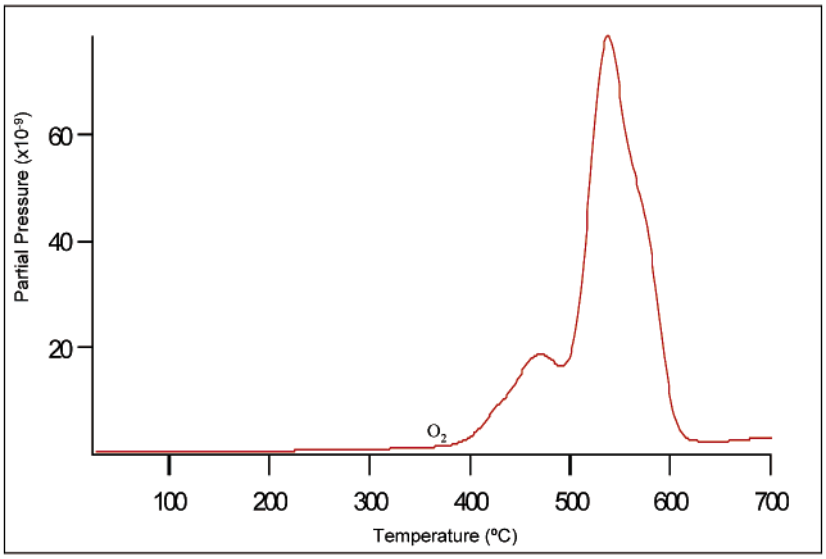

Figure 7. TPD−MS data for OMS-1 in a He atmosphere from 30 to 700 °C with a ramp of 10 °C/min.

2. Transformation Process of Mg−OL-1 Thin Films to Mg−OMS-1 Nanoribbons. The third step of the synthesis is to transform thin-film-like Mg−OL-1 material into nanoribbonlike Mg−OMS-1 material by hydrothermal heating. The formation of the nanoribbons of the layered structure from the thin-film sheets of the Mg−OL-1 precursor occurs at early stages of hydrothermal treatment. At this formation stage, the TEM data show that these Mg−OL-1 nanoribbons are oriented with [010] parallel to the major axis, indicating that they form by scission of the layered structure along the (100) planes. According to recent reports in the literature,[21] OL-1 material is a layered manganese oxide formed by edge-shared MnO_6 octahedra with mixed Mn(IV) and Mn(III) octahedra. During the hydrothermal heating, a transformation occurs from the layered structures to the tunnel structures that have corner-sharing MnO_6 octahedra. Some of the Mn(III) octahedra from the layers of the precursors may migrate into the interlayer region and become corner-sharing octahedra that assist in the formation of the "walls" of the tunnels. Typical bulk layered-structure materials from conventional syntheses consist of large platelike particles with profuse twinning and many dislocations.[1e,2b] Using these defective layered structural materials as precursors, the migrating Mn(III) octahedra from one crystal may easily interact with other octahedra that are nearby (within the large particle) and form "shared walls", resulting in discontinuous tunnels, twinned crystals, and large particles of OMS-1 materials. The Mg−OL-1 precursors prepared from TEA−OL-1 materials are thin-film-like and free of twins and dislocations. According to the TEM data, well-separated ribbons form from these thin-film precursor crystals and retain the

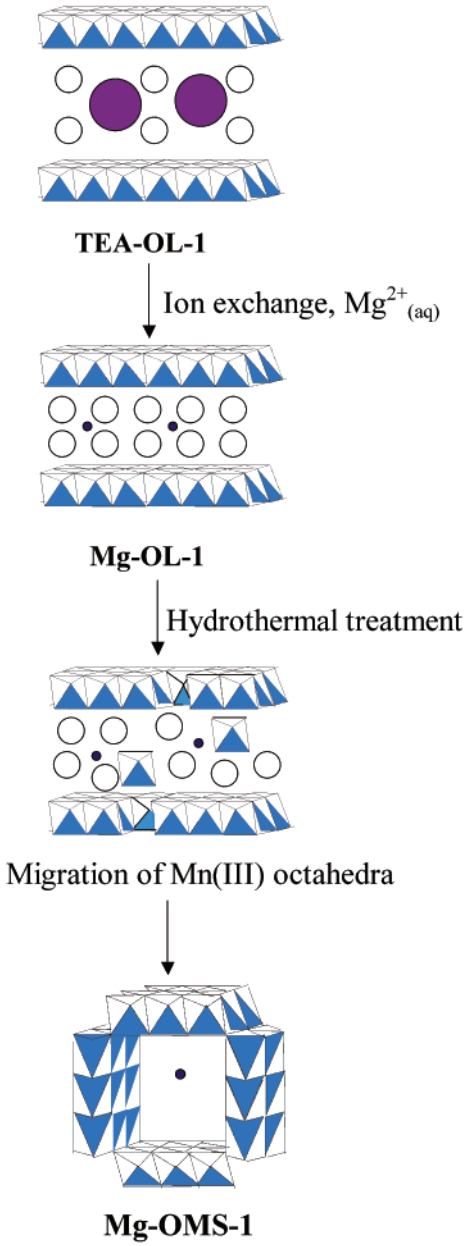

Figure 8. Schematic diagram of the transformation of TEA−OL-1 materials to Mg−OL-1 materials with ion-exchange methods and the transformation of Mg−OL-1 precursors to Mg−OMS-1 nanoribbons with hydrothermal treatment. The large solid spheres represent TEA cations. The small white spheres represent water molecules. The small solid spheres represent Mg cations.

buserite structure. Therefore, when the Mn(III) octahedra migrate into the interlayers in the structure of the fibrous buserite and build up "walls", the corner-shared MnO_6 octahedra are formed within the region of the original fiber. The interaction of one fiber with other ribbons is limited. A schematic diagram of the transformation process is shown in Figure 8.

3. Temperature and Time Effects on the Structural Transformation. The temperature and time of hydrothermal heating affect the structural transformation from the buserite precursor to the todorokite products. The transformation of Mg−OL-1 to Mg−OMS-1 should be an endothermic process due to bond dissociation. The transformation processes are accelerated by an increase in the hydrothermal treatment temperature. At lower temperatures such as 120 °C, the transformation from the buserite precursor to todorokite is not complete after 3 days. When the temperature is increased to 150 °C, the transformation is complete after heating for 40 h. At higher temperatures such as 200 °C, the transformation process is complete in 8 h. Longer heating leads to the formation of crystalline manganite phases.

4. Characterization of Mg−OMS-1 Nanoribbons. Todorokite-structured materials have two diagnostic peaks.[2] As suggested in the literature,[3c] a few layered materials with large cations, including Mg^{2+}, also show two peaks at similar positions in their XRD patterns, so the XRD results alone cannot be taken as diagnostic evidence of the presence of todorokite. To confirm the tunnel structure of the OMS-1 nanoribbons, further investigations were performed by ion exchange with Na^+. The distances between the interlayers of the layered-structure manganese oxides decrease when the original, large interlayer cations, such as Mg^{2+}, are exchanged by other cations, such as Na^+, because more water molecules are bound to Mg^{2+} ions than to Na^+ ions. The distance between the interlayers of Na−OL-1 is about 7.6 Å. Therefore, if the nanoribbons had a layered structure, the *d* spacings would decrease after the ion-exchange reaction. The XRD data show no change in the peak positions of the samples before and after the ion-exchange investigation. This evidence confirms the tunnel structure of OMS-1 nanoribbons. The TEM data also confirm that the nanoribbons have a long-range-ordered todorokite-type tunnel structure.

The average oxidation state (AOS) of manganese ions in OMS-1 nanoribbons is slightly higher than that in bulk materials reported in the literature.[3b] Compared with bulk OMS-1 material, nanoribbonlike OMS-1 material contains fewer Mg^{2+} cations because of the presence of more Mn^{4+}, as indicated by the higher AOS. The thermal stabilities of OMS-1 nanoribbons are similar to that of the bulk material, according to the TGA and TPD−MS data, which indicate that water and oxygen that are evolved are from the same sites in the structure.

The BET surface area of the nanoribbon sample is more than three times higher than that of the bulk Mg−OMS-1 material synthesized using conventional preparation methods.[22] The surface area is increased because of the smaller size of nanoribbonlike OMS-1 crystals.

5. Catalytic Application of Mg−OMS-1 Nanoribbons. The conversion in the oxidation of benzyl alcohol to benzaldehyde using Mg−OMS-1 nanoribbons as a catalyst is greatly increased. According to Son et al.,[18] the catalytic reaction follows a Mars−van Krevelen mechanism. The improvement of the performance of the nanoribbonlike catalyst compared to that of the bulk catalyst may be due to the smaller particle size with a resultant larger surface area for the Mg−OMS-1 material. The increase of the acidity of nanoribbonlike Mg−OMS-1 materials due to the neutral environment of synthesis as compared to the highly basic synthesis environment for conventional OMS-1 materials may be another possible reason for the improvement of their catalytic activity.[23] Further investigations on the mechanism of the catalytic reaction for nanoribbonlike Mg−OMS-1 are ongoing.

Conclusions

Mg−OMS-1 nanoribbons were synthesized using a preparation method consisting of three major steps: sol−gel synthesis of a layered TEA−manganese oxide precursor, ion exchange to prepare a Mg−OL-1 precursor, and a hydrothermal reaction to form Mg−OMS-1 nanoribbons. The thin-film-like Mg−OL-1 precursor with no twinning may play a key role in the transformation to the nanoribbonlike material. The nanoribbons form but retain the buserite structure at the beginning of the hydrothermal treatment. The structural transformation can be

accelerated by increasing the heating temperature. The well-formed nanoribbons have a uniform tunnel dimension and a long-range-ordered todorokite structure with nanoscale width and microscale length. The nanoribbonlike material is stable at temperatures of up to 500 °C. The surface area of these nanoribbons is far higher than that of bulk todorokite material. Conversion in the oxidation of benzyl alcohol to benzaldehyde has been increased from 2% using bulk Mg−OMS-1 material to 45% using nanoribbonlike Mg−OMS-1 material. The long-range-ordered 1D nanostructure could lead to new applications for manganese oxide octahedral molecular sieve materials and may improve their performance in widespread applications.

Acknowledgment. We acknowledge support by the Geosciences and Biosciences Division, Office of Basic Energy Sciences, Office of Science, United States Department of Energy. J. L. thanks Larry McCurdy for help with the TEM experiments. We also thank Dr. Franscis S. Galasso and Dr. Stephanie L. Brock for helpful discussions.

References and Notes

(1) (a) Turner, S.; Siegel, M. D.; Buseck, P. R. *Nature (London)* **1982**, *296*, 841, 842. (b) Burns, R. G.; Burns, V. M.; Stockman, H. W. *Am. Mineral.* **1983**, *68*, 972−980. (c) Golden, D. C.; Dixon, J. B.; Chen, C. C. *Clays Clay Miner.* **1986**, *34*, 511−520. (d) Bish, D. L.; Post, J. E. *Am. Mineral.* **1989**, *74*, 177−186. (e) Post, J. E.; Veblen, D. R. *Am. Mineral.* **1990**, *75*, 477−489. (f) Post, J. E. *Proc. Natl. Acad. Sci. U.S.A.* **1999**, *96*, 3447−3454.

(2) (a) Golden, D. C.; Chen, C. C.; Dixon, J. B. *Science (Washington, D.C.)* **1986**, *231*, 717−719. (b) Golden, D. C.; Chen, C. C.; Dixon, J. B. *Clays Clay Miner.* **1987**, *35*, 271−280. (c) Post, J. E.; Bish, D. L. *Am. Mineral.* **1988**, *73*, 861−869.

(3) (a) Shen, Y. F.; Zerger, R. P.; DeGuzman, R. N.; Suib, S. L.; McCurdy, L.; Potter, D. I.; O'Young, C. L. *Science (Washington, D.C.)* **1993**, *260*, 511−515. (b) Shen, Y. F.; Zerger, R. P.; DeGuzman, R. N.; Suib, S. L.; McCurdy, L.; Potter, D. I.; O'Young, C. L. *J. Chem. Soc., Chem. Commun.* **1992**, *17*, 1213, 1214. (c) Shen, Y. F.; Suib, S. L.; O'Young, C. L. *J. Am. Chem. Soc.* **1994**, *116*, 11020−11029. (d) Tian, Z.-R.; Yin, Y.-G.; Suib, S. L. *Chem. Mater.* **1997**, *9*, 1126−1133.

(4) Feng, Q.; Kanoh, H.; Miyai, Y.; Ooi, K. *Chem. Mater.* **1995**, *7*, 1722−1727.

(5) (a) Suib, S. L. *Curr. Opin. Solid State Mater. Sci.* **1998**, *3*, 63−70. (b) Brock, S. L.; Duan, N.; Tian, Z. R.; Giraldo, O.; Zhou, H.; Suib, S. L. *Chem. Mater.* **1998**, *10*, 2619−2628. (c) Luo, J.; Zhang, Q.; Suib, S. L. *Inorg. Chem.* **2000**, *39*, 741−747.

(6) (a) Nitta, M. *Appl. Catal.* **1984**, *9*, 151−176. (b) Wong, S. T.; Cheng, S. *Inorg. Chem.* **1992**, *31*, 1165−1172. (c) Pereira-Ramos, J. P.; Badour, R.; Bach, S.; Baffier, N. *Solid State Ionics* **1992**, *701*, 3−56. (d) Bach, S.; Pereira-Ramos, J. P.; Baffier, N. *Electrochim. Acta* **1993**, *38*, 1695−1700. (e) Armstrong, A. R.; Bruce, P. G. *Nature (London)* **1996**, *381*, 499−500. (f) Shen, Y. F.; Suib, S. L.; O'Young, C. L. *J. Catal.* **1996**, *161*, 115−122.

(7) (a) Marquez, M.; Larsen, G.; Haller, G. L. *J. Phys. Chem.* **1992**, *96*, 4145−4149. (b) Wu, C. G.; Bein, T. *Science (Washington, D.C.)* **1994**, *264*, 1757−1759.

(8) (a) Martin, C. R. *Chem. Mater.* **1996**, *8*, 1739−1746. (b) Jirage, K. B.; Hulteen, J. C.; Martin, C. R. *Science (Washington, D.C.)* **1997**, *278*, 655−658. (c) Cepak, V. M.; Martin, C. R. *Chem. Mater.* **1999**, *11*, 1362−1367.

(9) Alivisatos, A. P. *Science (Washington, D.C.)* **1996**, *271*, 933−937.

(10) (a) Fan, S.; Chapline, M. G.; Franklin, N. R.; Tombler, T. W.; Cassell, A. M.; Dai, H. *Science (Washington, D.C.)* **1999**, *283*, 512−514. (b) Hu, J.; Ouyang, M.; Yang, P.; Lieber, C. M. *Nature (London)* **1999**, *399*, 48−51.

(11) (a) Holmes, J. D.; Johnston, K. P.; Doty, R. C.; Korgel, B. A. *Science (Washington, D.C.)* **2000**, *287*, 1471−1473. (b) Kondo, Y.; Takayanagi, K. *Science (Washington, D.C.)* **2000**, *289*, 606−608.

(12) (a) Huang, M. H.; Mao, S.; Feich, H.; Yan, H.; Wu, Y.; Kind, H.; Weber, E.; Russo, R.; Yang P. *Science (Washington, D.C.)* **2001**, *292*, 1897−1899. (b) Tosatti, E.; Prestipino, S.; Kostlmeier, S.; Dal Corso, A.; Di Tolla, F. D. *Science (Washington, D.C.)* **2001**, *291*, 288−290.

(13) (a) Brock, S. L.; Sanabria, M.; Suib, S. L. *J. Phys. Chem. B* **1999**, *103*, 7416−7428. (b) Brock, S. L.; Sanabria, M.; Nair, J.; Suib, S. L.; Ressler, T. *J. Phys. Chem. B* **2001**, *105*, 5404−5410. (c) Gao, Q.; Giraldo, O.; Tong, W.; Suib, S. L. *Chem. Mater.* **2001**, *13*, 778−786.

(14) (a) Giraldo, O.; Brock, S. L.; Marquez, M.; Suib, S. L.; Hillhouse, H.; Tsapatsis, M. *Nature (London)* **2000**, *405*, 38. (b) Girlado, O.; Marquez, M.; Brock, S. L., Suib, S. L.; Hillhouse, H.; Tsapatsis, M. *J. Am. Chem. Soc.* **2000**, *122*, 12158−12163. (c) Girlado, O.; Brock, S. L.; Willis, W. S.; Marquez, M.; Suib, S. L. *J. Am. Chem. Soc.* **2000**, *122*, 9930, 9931.

(15) Xia, G.-G.; Tong, W.; Tolentino, E. N.; Duan, N.-G.; Brock, S. L.; Wang, J.-Y.; Suib, S. L.; Ressler, T. *Chem. Mater.* **2001**, *13*, 1585−1592.

(16) Yang, X.; Kanoh, H.; Tang, W.; Liu, Z.-H.; Ooi, K. *Chem. Lett.* **2000**, 1192, 1193.

(17) Cai, J.; Liu, J.; Willis, W. S.; Suib, S. L. *Chem. Mater.* **2001** *13*, 2413−2422.

(18) Son, Y.-C.; Makwana, V. D.; Howell, A. R.; Suib, S. L. *Angew. Chem., Int. Ed.* **2001**, *40*, 4280−4283.

(19) Brinker, C. J.; Scherer, G. W. *Sol−Gel Science;* Academic Press: New York, 1990.

(20) (a) Bach, S.; Henry, M.; Baffier, N.; Livage, J. *J. Solid State Chem.* **1990**, *88*, 325−333. (b) Ching, S.; Landrigan, J. A.; Jorgensen, M. L.; Duan, N.; Suib, S. L.; O'Young, C.-L. *Chem. Mater.* **1995**, *7*, 1604−1606. (c) Le Goff, P.; Baffier, N. *Solid State Ionics* **1993**, *61*, 309−315.

(21) (a) Drits, V. A.; Silvester, E.; Gorshkov, A. I.; Manceau, A. *Am. Mineral.* **1997**, *82*, 946−961. (b) Silvester, E.; Manceau, A.; Drits, V. A. *Am. Mineral.* **1997**, *82*, 962−978.

(22) Liu, J.; Hincapie, B. O.; Della Vecchia, K. M.; Suib, S. L.; Bushmich, S. L.; Wu, A.; Hursey, F. X. Submitted for publication.

(23) Makwana, V. D.; Son, Y.-C.; Howell, A. R.; Suib, S. L. Submitted for publication.